


Fourfold metallic-mean quasicrystals as aperiodic approximants of the square lattice

Joichiro Nakakura,¹ Primož Zihelr^{2,3} , and Tomonari Dotera^{1,*} 

¹*Department of Physics, Kindai University, Higashiosaka, Osaka 577-8502, Japan*

²*Faculty of Mathematics and Physics, University of Ljubljana, Jadranska 19, SI-1000 Ljubljana, Slovenia*

³*Jožef Stefan Institute, Jamova 39, SI-1000 Ljubljana, Slovenia*



(Received 16 March 2023; revised 18 June 2024; accepted 8 July 2024; published 19 July 2024)

By proposing a family of two-lengthscale quasicrystalline tilings characterized by even-numbered metallic-mean inflation ratios, we extend the recently introduced notion of aperiodic approximants of triangular and honeycomb lattices to square crystals. The proposed family originates in the eightfold Ammann-Beenker and fourfold Harriss quasicrystals and is based on sets of two square tiles and a parallelogram. We elaborate the higher-dimensional representation of the new tilings and we show that at large inflation ratios they tend to the square lattice just like their triangular and hexagonal counterparts.

DOI: [10.1103/PhysRevB.110.014108](https://doi.org/10.1103/PhysRevB.110.014108)

I. INTRODUCTION

The science of quasicrystals stems from the large body of work on icosahedral [1–3], decagonal [4,5], octagonal, and dodecagonal quasicrystals [6–9]. At the same time, it is long known that these “forbidden rotational symmetries” are not required for generic aperiodic structures in the context of crystallography [10–12]. It is easy to generate infinitely many types of one-dimensional aperiodic sequences using substitution rules such as the Fibonacci lattice and in them the rotational symmetry is irrelevant. By superposing two one-dimensional Fibonacci lattices in perpendicular directions, the square Fibonacci tiling can be constructed as an example of a quasicrystalline structure with fourfold symmetry [13]; such a quasicrystal was observed in a C₆₀ monolayer deposited on the twofold surface of an AlPdMn quasicrystal [14]. A different fourfold quasicrystalline tiling was constructed by Harriss and Lamb two decades ago [15] and yet another example of an allowed symmetry in an aperiodic pattern is the recently proposed golden-mean tiling with sixfold symmetry, which is usually regarded as a strong indication of hexagonal periodic positional order [16–18].

Hexagonal quasicrystals were first associated with the metallic means by the bronze-mean tiling [19]. This tiling is of physical relevance because it was observed in numerical simulations of ensembles of particles interacting with a suitable pair potential such as the two-lengthscale hard-core/square-shoulder repulsion [19], as well as in density-functional theory [20]. The bronze-mean pattern was later generalized to an infinite two-parameter family of hexagonal quasicrystalline tilings. This family includes tilings characterized by inflation factors that are metallic means of multiples of 3 [21], the metallic means

$$\beta_k = \frac{k + \sqrt{k^2 + 4}}{2} = k + \frac{1}{k + \frac{1}{k + \dots}} \quad (1)$$

being the positive solutions of the quadratic equation $x^2 - kx - 1 = 0$, where k is a natural number. The most famous metallic mean is the golden mean at $k = 1$ associated with the Penrose tiling and icosahedral quasicrystals. Also well studied is the silver mean at $k = 2$, which underlies the Ammann-Beenker tiling, and the inflation factor of the Harriss tilings [15], which too are of the Ammann-Beenker type, is the fourth metallic mean (although this was not explicitly pointed out). In turn, the fourth metallic mean happens to be the inflation ratio of icosahedral quasicrystals.

The conceptual significance of the geometric construction leading to the metallic-mean hexagonal quasicrystalline tilings is in the systematic method for generation of sequences of quasicrystalline (or incommensurate) tilings in two dimensions. Recently, it was discovered that new metallic-mean tilings serve as aperiodic approximants, bridging incommensurate modulated structures and quasicrystals [18]. As such, they are valuable tools for studying domain wall structures in polymers and colloidal systems. Interestingly, the diffraction peaks of the twin-boundary superstructures in systems of colloidal particles interacting with the Lennard-Jones–Gauss potential [22] can be analyzed using the higher-dimensional quasicrystal theory of the metallic-mean aperiodic approximants. This shows that these approximants can significantly contribute to the understanding of complex structures observed in condensed matter.

The objectives of this paper are (i) to demonstrate how the approach introduced in Ref. [21] can be generalized to quasicrystalline patterns of other types of rotational symmetries and (ii) to provide further support for the notion of aperiodic approximants. To this end, we use the above approach to explore the fourfold (square) quasicrystalline patterns with various inflation factors by starting with the Ammann-Beenker tiling; our results also include the Harriss tilings. We show that the inflation factors of the fourfold quasicrystalline patterns comprise all even-numbered metallic means. Furthermore, we observe that the diagonal Ammann lines of the Harriss canonical II tiling form the Fibonacci sequence. These findings illustrate the close connection between

*Contact author: dotera@phys.kindai.ac.jp

the family of fourfold tilings proposed here and the previously explored two-dimensional quasicrystalline structures.

This paper is organized as follows. In Sec. II, we start from the well-known Ammann-Beenker tiling and we first generalize it to the fourth metallic-mean tiling, namely the Harriss canonical II tiling, and then to all other even-numbered metallic-mean tilings, focusing on their properties in the limit where $k \rightarrow \infty$. In Sec. III, we construct a higher-dimensional representation to elucidate how to generate the window in the perpendicular space and we compute the Fourier transform. Section IV concludes the paper.

II. GENERALIZED AMMANN-BEENKER TILING

Our even-numbered metallic-mean tilings characterized by fourfold rotational symmetry, two lengthscales, and three types of tiles are derived from the Ammann-Beenker and the Harriss canonical II tilings and we first review these two patterns.

A. Ammann-Beenker tiling

A quasicrystalline tiling is conveniently defined by the subdivision rules and those for the Ammann-Beenker tiles are shown in Figs. 1(a) and 1(b) [12]. The black and the white squares indicate the symmetry of the subdivision rules. The rhombus has a twofold rotational symmetry, but the subdivision inside the square is directional. Also drawn on edges are arrows that allow the tiles to fit together only if the orientations of arrows match. The arrows are related to the black and white squares in that each black square is a source of two arrows.

To see how the matching rules generate quasiperiodicity, we resort to the Ammann lines consisting of segments that decorate each tile [Fig. 2(a)] [2,3,23,24]. By requiring that the Ammann lines are straight, one disposes of the matching conditions imposed by the above black and white markings, arrows, or notches. The Ammann lines for the Ammann-Beenker tiling define four sets of parallel lines referred to as grids. In each grid, the spacings between adjacent lines constitute a quasiperiodic sequence of a long and short length denoted by L and S and the substitution rules for the sequence read $L \rightarrow SSL$ and $S \rightarrow SL$ or in matrix form

$$\begin{pmatrix} L \\ S \end{pmatrix} \rightarrow \begin{pmatrix} 1 & 2 \\ 1 & 1 \end{pmatrix} \begin{pmatrix} L \\ S \end{pmatrix}. \quad (2)$$

The eigenvalue of the substitution matrix is the silver mean $\beta_2 = 1 + \sqrt{2}$ and the ratio of the grid spacings is given by $L/S = \sqrt{2}$. The Ammann-Beenker tiling satisfies the ‘‘alternation condition’’ [9,25] requiring that, along any Ammann line, the two orientations of the rhombi must alternate irrespective of whether there is a square between them or not. This condition is enforced by the arrows at the edges, which must match.

The Ammann-Beenker tiling contains square tiles of two orientations as emphasized in Fig. 1: Fig. 1(c) is the same as Fig. 1(b) except that it is rotated by 45° . If the edge lengths of the two squares are different, say A in the square in Fig. 1(b) and B in that in Fig. 1(c), the octagonal symmetry is lowered to the square symmetry. Upon subdivision, the lengths A_i and

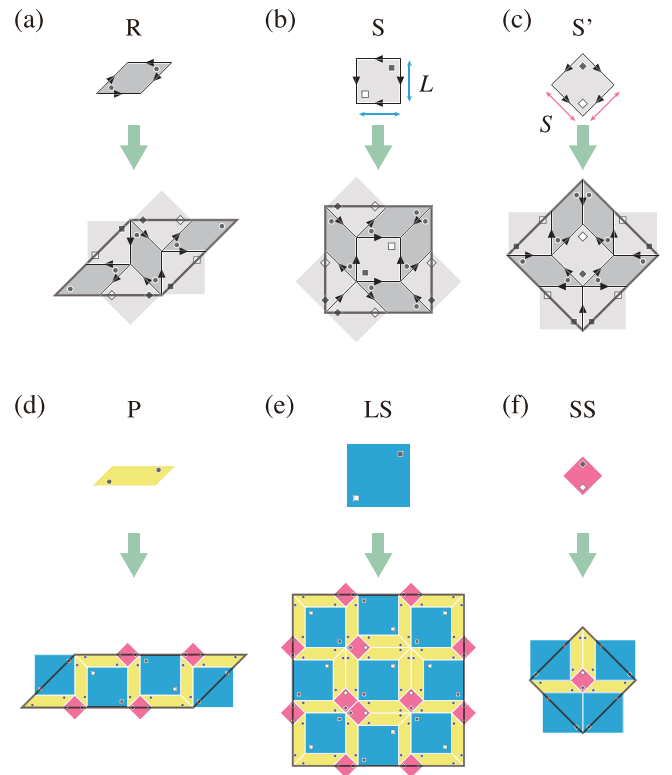


FIG. 1. Subdivision schemes for the Ammann-Beenker (silver mean) tiling and the Harriss canonical II (fourth metallic-mean) tiling. The Ammann-Beenker tiles: (a) 45° rhombus (R) and (b) square (S). Panel (c) shows the square tile (S') rotated by 45° with respect to S for comparison with the corresponding Harriss canonical II tile; the edge lengths of the S and S' tiles denoted by L and S , respectively, are the same. The tile matching rules are shown by arrows on the edges of the Ammann-Beenker tiling and each black square mark is a source of arrows. The Harriss canonical II tiles: (d) parallelogram, (e) large square, and (f) small square; in these three panels, arrows are not shown for clarity.

B_i of the i th generation transform as

$$\begin{pmatrix} A_{i+1} \\ B_{i+1} \end{pmatrix} = \begin{pmatrix} 1 & \sqrt{2} \\ \sqrt{2} & 1 \end{pmatrix} \begin{pmatrix} A_i \\ B_i \end{pmatrix}. \quad (3)$$

The positive eigenvalue of the matrix is the silver mean $\beta_2 = 1 + \sqrt{2}$ and the corresponding edge ratio is $A/B = 1$; this choice gives the Ammann-Beenker tiling.

B. Square Harriss canonical II tiling

Now we describe the square Harriss canonical II (fourth metallic-mean) tiling, which has several elegant properties [15]. This tiling consists of three types of tiles: parallelogram (P), large square (LS), and small square (SS) shown in Figs. 1(d), 1(e) and 1(f), respectively. The subdivision rules for the P and LS tiles are different from those of the parent R and S tiles of the Ammann-Beenker tiling, but the subdivision rule for the Harriss SS tile and the Ammann-Beenker S' tile are topologically identical [Figs. 1(c) and 1(f)]. The matching rules of the Harriss tiles [represented by black and white squares in Figs. 1(d)–1(f); arrows are not displayed

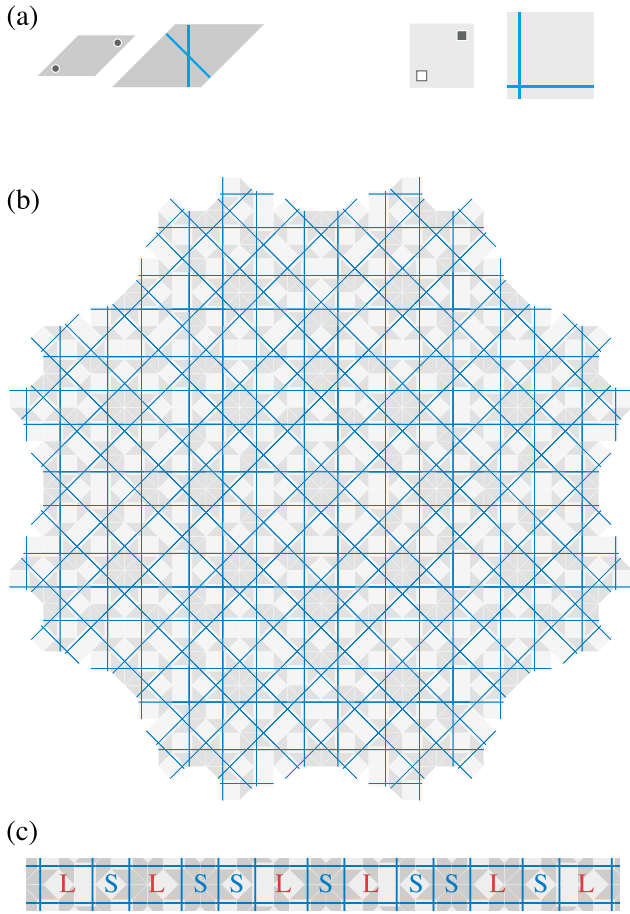


FIG. 2. Ammann lines: (a) Ammann decoration of the Ammann-Beenker tiles, (b) Ammann lines for the third generation tiling showing the octagonal point symmetry configuration with respect to the center, and (c) aperiodic sequence of the two spacings between the lines illustrated by the horizontal cut through the center of the pattern in panel (b).

for clarity] are the same as those of the Ammann-Beenker tiling. The tiling also satisfies the alternation condition, since it is required by the arrow matching rules. The lengths of long (A) and short (B) sides of quadrilaterals transform by a nonsymmetric matrix as

$$\begin{pmatrix} A_{i+1} \\ B_{i+1} \end{pmatrix} = \begin{pmatrix} 3 & 2\sqrt{2} \\ \sqrt{2} & 1 \end{pmatrix} \begin{pmatrix} A_i \\ B_i \end{pmatrix}. \quad (4)$$

The characteristic equation reads $x^2 - 4x - 1 = 0$ and the positive eigenvalue is the fourth metallic mean $\beta_4 = 2 + \sqrt{5} = \tau^3$, where τ is the golden mean $(1 + \sqrt{5})/2$. The self-similar edge length ratio is given by $A/B = \tau\sqrt{2} \cong 2.288$.

The Ammann lines for the Harriss canonical II tiling give four sets of grids (parallel lines) as illustrated in Figs. 3(a)–3(c). In each grid, the sequence of spacing between successive lines is a quasiperiodic sequence of two lengths. As we now show, the horizontal (0°) and vertical (90°) sequences obey the $\beta_4 = \tau^3$ scaling, whereas the diagonal (45° and 135°) sequences obey the τ scaling, which implies that the latter sequence is the one-dimensional Fibonacci lattice. The

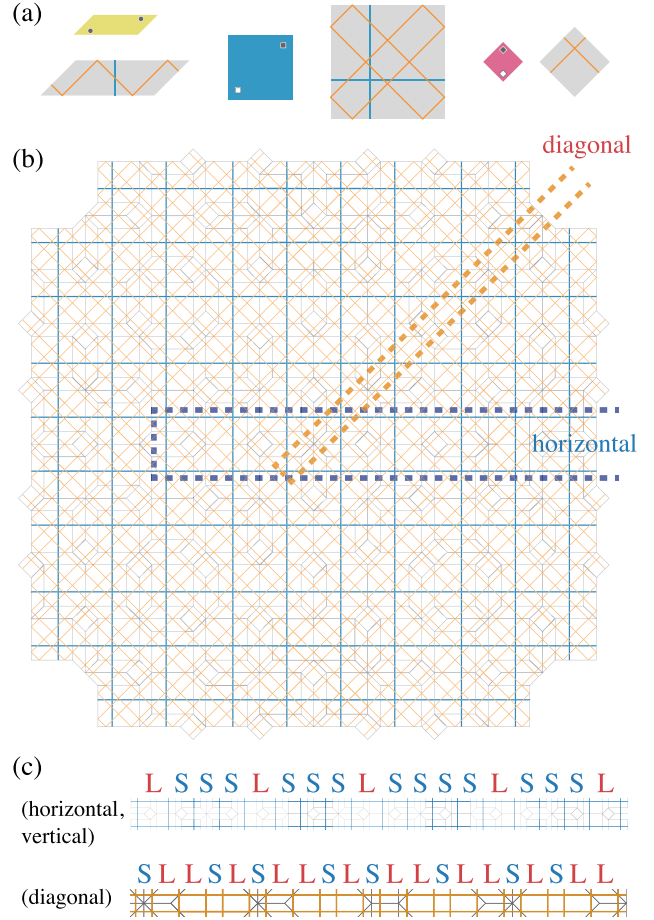


FIG. 3. Ammann line decorations of the square Harriss canonical II tiling: (a) tile decorations of Ammann lines for tiles, with horizontal (0°) and vertical (90°) lines shown in blue and diagonal (45° and 135°) lines in brown, (b) square symmetry configuration around its center, and (c) aperiodic two-lengthscale LS sequence (top: horizontal and vertical direction; bottom: diagonal direction); the diagonal directions give the Fibonacci LS sequence.

substitution rules for long (L) and short (S) intervals are

$$L \rightarrow SSSSL, \quad S \rightarrow SSSL \quad (5)$$

for the horizontal and vertical directions and

$$L \rightarrow LSLSL, \quad S \rightarrow LSL \quad (6)$$

for the diagonal directions. In matrix form, the substitution rule for the horizontal and vertical sequences reads

$$\begin{pmatrix} L \\ S \end{pmatrix} \rightarrow \begin{pmatrix} 1 & 4 \\ 1 & 3 \end{pmatrix} \begin{pmatrix} L \\ S \end{pmatrix}, \quad (7)$$

where the ratio of the spacings is given by $L/S = \sqrt{5} - 1 \cong 1.236$. The substitution rules for the diagonal sequences are

$$\begin{pmatrix} L \\ S \end{pmatrix} \rightarrow \begin{pmatrix} 3 & 2 \\ 2 & 1 \end{pmatrix} \begin{pmatrix} L \\ S \end{pmatrix} = \begin{pmatrix} 1 & 1 \\ 1 & 0 \end{pmatrix}^3 \begin{pmatrix} L \\ S \end{pmatrix} \quad (8)$$

and the ratio of the spacings is given by $L/S = \tau \cong 1.618$. If we only look at diagonal ones, we observe the square Fibonacci tiles [13]. This situation is reminiscent of the

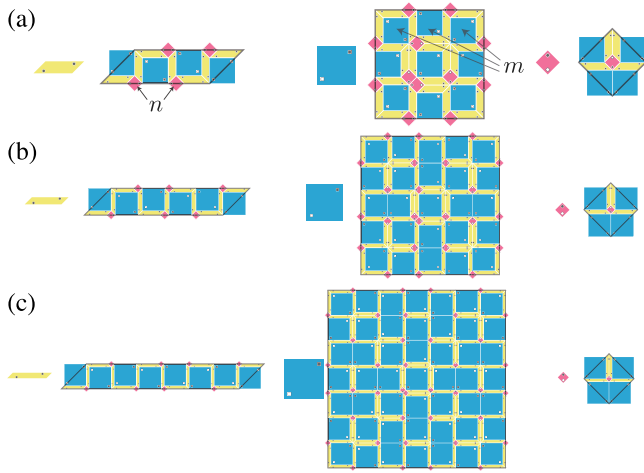


FIG. 4. Subdivision schemes for the parallelogram (P), large-square (LS), and small-square (SS) tile of the even-numbered metallic-mean tilings: (a) $k = 4$ ($n = 2, m = 3$), (b) $k = 6$ ($n = 3, m = 5$), and (c) $k = 8$ ($n = 4, m = 7$). Each panel contains all three tiles decorated by the white and black squares together with their enlarged copies showing subdivision into the next-generation tiles deflated by a factor of β_k . The subdivisions are characterized by the numbers of next-generation SS and LS tiles along the edges of P and LS tiles denoted by n and m , respectively; this is shown in panel (a).

primitive icosahedral quasicrystals, where the twofold axis obeys the τ^3 scaling, whereas the three- and fivefold axis obeys the τ scaling.

C. Even-numbered metallic-mean tilings

Now we introduce a more general form of subdivision scheme for the set of tiles containing parallelograms (P), large squares (LS), and small squares (SS), which serve as a basis of a family of fourfold aperiodic tilings. This scheme is parametrized by the numbers of next-generation SS and LS tiles along the edge of the P and LS tiles denoted by n and m , respectively, as illustrated in Fig. 4(a).

As before, we begin the analysis by examining the transformation of the lengths upon subdivision; A and B again stand for the edges of the LS and the SS tile, respectively. The transformation reads

$$\begin{pmatrix} A_{i+1} \\ B_{i+1} \end{pmatrix} = \begin{pmatrix} m & \sqrt{2}n \\ \sqrt{2} & 1 \end{pmatrix} \begin{pmatrix} A_i \\ B_i \end{pmatrix}, \quad (9)$$

where m and n are natural numbers; note that for $m = n = 1$ and $m = 3, n = 2$ this transformation reduces to Eqs. (3) and (4), respectively. The characteristic equation reads

$$\lambda^2 - (m+1)\lambda + m - 2n = 0. \quad (10)$$

The positive eigenvalue of the matrix is

$$\lambda = \frac{m+1 + \sqrt{(m-1)^2 + 8n}}{2} \quad (11)$$

and the corresponding eigenvector gives the self-similar length ratio

$$\phi = \frac{A}{B} = \frac{m-1 + \sqrt{(m-1)^2 + 8n}}{2\sqrt{2}}. \quad (12)$$

TABLE I. Inflation factors for three-tile fourfold aperiodic tilings defined by the subdivision scheme in Fig. 4. The even-numbered metallic means are typeset in boldface.

$m \setminus n$	1	2	3	4
n	$1 + \sqrt{2}$	$\frac{3+\sqrt{17}}{2}$	$2 + \sqrt{7}$	$\frac{5+\sqrt{41}}{2}$
$n+1$	3	$2 + \sqrt{5}$	$\frac{5+\sqrt{33}}{2}$	$3 + 2\sqrt{3}$
$n+2$	$2 + \sqrt{3}$	5	$3 + \sqrt{10}$	$\frac{7+\sqrt{57}}{2}$
$n+3$	$\frac{5+\sqrt{17}}{2}$	$3 + 2\sqrt{2}$	7	$4 + \sqrt{17}$

Also of interest are the numbers of long (A) and short (B) edges n_i^A and n_i^B , respectively, which transform according to

$$\begin{pmatrix} n_{i+1}^A \\ n_{i+1}^B \end{pmatrix} = \begin{pmatrix} m & \sqrt{2} \\ \sqrt{2}n & 1 \end{pmatrix} \begin{pmatrix} n_i^A \\ n_i^B \end{pmatrix}, \quad (13)$$

and the eigenvector of the transform defines the number ratio

$$\psi = \frac{n^A}{n^B} = \frac{m-1 + \sqrt{(m-1)^2 + 8n}}{2\sqrt{2}n}. \quad (14)$$

In Table I, the inflation factors given in Eq. (11) are listed for n between 1 and 4 and m between n and $n+3$. Remarkably, we notice that the specific choice

$$n = k/2, \quad m = k-1 \quad (15)$$

in Eq. (10), namely $m-2n = -1$, leads to metallic-mean inflation factors $\lambda = \beta_k$ for $k = 2, 4, 6, \dots$. These special cases lie on the diagonal of Table I; in particular, the silver and the fourth metallic mean correspond to $n = 1, m = 1$ and $n = 2, m = 3$, respectively. Also intriguing are the tilings with $m = 2n$ characterized by integer inflation factors equal to $2n+1$, which implies that these tilings are periodic. Since they appear as special cases within a family of aperiodic tilings, their periodicity is accidental just like in their periodic three-tile hexagonal counterparts [19].

Accordingly, the self-similar length ratio of the even-numbered metallic-mean tilings reads

$$\phi = \frac{k-2 + \sqrt{k^2+4}}{2\sqrt{2}} \quad (16)$$

and the ratio of the numbers of long and short edges is

$$\psi = \frac{k-2 + \sqrt{k^2+4}}{\sqrt{2}k}. \quad (17)$$

For $k = 2$ (the silver mean) alone, we have $\phi = \psi = 1$; otherwise, these two ratios are not the same. Therefore, whereas the Ammann-Beenker $k = 2$ tiling can be generated by inflation rules involving just two prototiles (because in this special case the SS and the LS tile coincide), all other even-numbered metallic-mean tilings introduced here are based on inflation rules involving three prototiles. Figures 5(a)–5(c) show the second-generation $k = 4, 6$, and 8 tilings, respectively, illustrating their fourfold symmetry and the characteristic slithering displacements of the LS tiles in each horizontal and vertical lane, which stems from the alternation condition. Also evident from this sequence is the increasing dominance of area

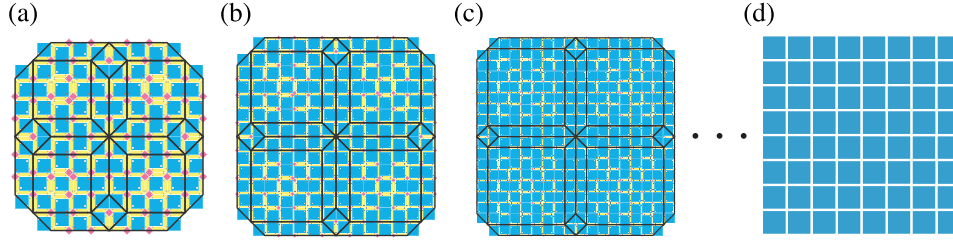


FIG. 5. Even-numbered metallic-mean aperiodic tilings with fourfold symmetry. Second-generation tilings with (a) the fourth metallic mean $k = 4$ ($n = 2, m = 3$), (b) the sixth metallic mean $k = 6$ ($n = 3, m = 5$), (c) the eighth metallic mean $k = 8$ ($n = 4, m = 7$), and (d) $k \rightarrow \infty$, respectively, with the first-generation fundamental motif outlined in black. Panel (d) shows a patch of the $k \rightarrow \infty$ tiling, which is a periodic square lattice arewisely dominated by the LS tiles.

covered by the LS tiles as k is increased and in Fig. 5(d) we plot the periodic square lattice as the $k \rightarrow \infty$ limiting case.

By inspecting the patterns in Fig. 5, we find that the numbers of SS, LS, and P tiles in the $(i + 1)$ th generation denoted by SS_{i+1} , LS_{i+1} , and P_{i+1} , respectively, are related to those in the i th generation by

$$\begin{pmatrix} SS_{i+1} \\ LS_{i+1} \\ P_{i+1} \end{pmatrix} = \begin{pmatrix} 1 & 2n^2 & n \\ 2 & m^2 & m \\ 4 & 4nm & 2n + m \end{pmatrix} \begin{pmatrix} SS_i \\ LS_i \\ P_i \end{pmatrix}. \quad (18)$$

For the even-numbered metallic-mean tilings, Eq. (15) gives

$$\begin{pmatrix} SS_{i+1} \\ LS_{i+1} \\ P_{i+1} \end{pmatrix} = \begin{pmatrix} 1 & k^2/2 & k/2 \\ 2 & (k-1)^2 & k-1 \\ 4 & 2k(k-1) & 2k-1 \end{pmatrix} \begin{pmatrix} SS_i \\ LS_i \\ P_i \end{pmatrix}. \quad (19)$$

The positive eigenvalue of this matrix is β_k^2 and the corresponding eigenvector is

$$\left(\frac{1}{2} - \frac{k}{4(\beta_k + 1)}, \frac{\beta_k}{2(\beta_k + 1)}, 1 \right). \quad (20)$$

For $k \rightarrow \infty$, the fractions of tiles $SS : LS : P$ converge to $1/7 : 2/7 : 4/7$. On the other hand, in this limit the areas of SS and P tiles go to zero compared to that of LS because the length ratio given by Eq. (16) diverges. We conclude that, in the limit of $k \rightarrow \infty$, the sequence of the even-numbered metallic-mean tilings reduces to the periodic square lattice composed of the LS tiles alone as depicted in Fig. 5(d).

III. HIGHER-DIMENSIONAL REPRESENTATION

After constructing the three-tile aperiodic lattices with fourfold rotational symmetry using the subdivision rule, we turn to their higher-dimensional description.

A. Projection matrices

Like in the sixfold aperiodic tilings [21], we search for a four-dimensional noncubic superspace lattice that will produce our fourfold tilings upon projection onto the physical space. We denote the orthonormal basis vectors of the superspace by \mathbf{e}_i , $i = 1, 2, 3, 4$, where $\mathbf{e}_i \cdot \mathbf{e}_j = \delta_{ij}$ and δ_{ij} is the Kronecker delta. The points of the superspace lattice are defined by

$$\mathbf{r} = \sum_{i=1}^4 n_i \mathbf{a}_i \equiv \sum_{i=1,3} n_i \mathbf{a}_e + \sum_{i=2,4} n_i \mathbf{c}_e, \quad (21)$$

where n_i ($i = 1, 2, 3, 4$) are integers, whereas a and c are lattice constants.

The next entity needed are the projection operators. Parametrized by ℓ , the projection operator onto the physical space is given by

$$P^{\parallel} = \frac{1}{2(\ell^2 + 1)} \begin{pmatrix} 2\ell^2 & \sqrt{2}\ell & 0 & -\sqrt{2}\ell \\ \sqrt{2}\ell & 2 & \sqrt{2}\ell & 0 \\ 0 & \sqrt{2}\ell & 2\ell^2 & \sqrt{2}\ell \\ -\sqrt{2}\ell & 0 & \sqrt{2}\ell & 2 \end{pmatrix} \quad (22)$$

so that $(P^{\parallel})^2 = P^{\parallel}$ and the corresponding projection operator onto the perpendicular space is

$$P^{\perp} = \frac{1}{2(\ell^2 + 1)} \begin{pmatrix} 2 & -\sqrt{2}\ell & 0 & \sqrt{2}\ell \\ -\sqrt{2}\ell & 2\ell^2 & -\sqrt{2}\ell & 0 \\ 0 & -\sqrt{2}\ell & 2 & -\sqrt{2}\ell \\ \sqrt{2}\ell & 0 & -\sqrt{2}\ell & 2\ell^2 \end{pmatrix} \quad (23)$$

so that $(P^{\perp})^2 = P^{\perp}$ and $P^{\parallel} + P^{\perp} = \mathbf{1}$. We note that P^{\parallel} and P^{\perp} with different ℓ are not orthogonal.

The projection operators allow us to define the primitive lattice vectors in the physical and in the perpendicular space given by $\mathbf{a}_i^{\parallel} \equiv P^{\parallel} \mathbf{a}_i$ and $\mathbf{a}_i^{\perp} \equiv P^{\perp} \mathbf{a}_i$, respectively. The lengths of the primitive lattice vectors are

$$|\mathbf{a}_{\text{odd}}^{\parallel}| = a\ell \sqrt{\frac{1}{\ell^2 + 1}}, \quad (24)$$

$$|\mathbf{a}_{\text{even}}^{\parallel}| = c\sqrt{\frac{1}{\ell^2 + 1}}, \quad (25)$$

$$|\mathbf{a}_{\text{odd}}^{\perp}| = a\sqrt{\frac{1}{\ell^2 + 1}}, \quad (26)$$

and

$$|\mathbf{a}_{\text{even}}^{\perp}| = c\ell \sqrt{\frac{1}{\ell^2 + 1}}, \quad (27)$$

and their relative orientations are shown in Fig. 6.

Now the main issue to be resolved is how to choose the two parameters ℓ and a/c so as to reconstruct our fourfold

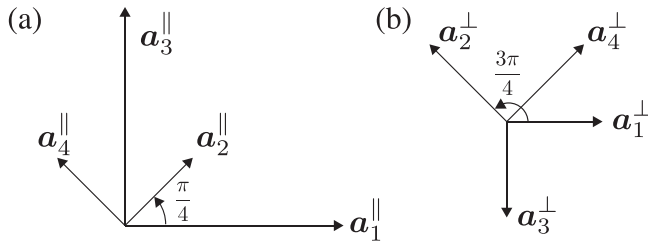


FIG. 6. Physical-space basis vectors \mathbf{a}_j^{\parallel} ($j = 1, 2, 3, 4$) and perpendicular-space basis vectors \mathbf{a}_j^{\perp} ($j = 1, 2, 3, 4$).

even-numbered metallic-mean tilings. In order to obtain a compact window, we fix the ratios of the lengths of the odd and the even primitive vectors in physical and perpendicular spaces by setting

$$\frac{|\mathbf{a}_{\text{odd}}^{\parallel}|}{|\mathbf{a}_{\text{even}}^{\parallel}|} = \frac{a\ell}{c} = \phi, \quad \frac{|\mathbf{a}_{\text{even}}^{\perp}|}{|\mathbf{a}_{\text{odd}}^{\perp}|} = \frac{c\ell}{a} = \psi, \quad (28)$$

so that

$$\frac{a}{c} = \sqrt{\frac{\phi}{\psi}}, \quad \ell = \sqrt{\phi\psi}. \quad (29)$$

In the even-numbered metallic-mean tilings,

$$\frac{a}{c} = \sqrt{\frac{k}{2}}, \quad \ell = \frac{k-2 + \sqrt{k^2+4}}{2\sqrt{k}}. \quad (30)$$

The ratios of the lengths of basis vectors in both spaces and the other parameters of interest are listed in Table II.

B. Local vertex configurations and windows in perpendicular space

As a parent pattern of our even-numbered metallic-mean tilings, the Ammann-Beenker tiling consists of six types of vertex configurations, whereas in the Harriss canonical II tiling as its immediate generalization there are nine types

TABLE II. Inflation factor, ratio of lattice constants c/a , ℓ , length ratio ϕ , and ratio of long and short edges ψ for the even-numbered metallic-mean tilings with $k = 2, 4, 6, 8$, and ∞ ; the exact values are complemented by the approximate ones for easier comparison.

k	2	4	6	8	...	∞
β_k	$1 + \sqrt{2}$ 2.414	$2 + \sqrt{5}$ 4.236	$3 + \sqrt{10}$ 6.162	$4 + \sqrt{17}$ 8.123	...	∞
a/c	1	$\sqrt{2}$	$\sqrt{3}$	2	...	∞
ℓ	1	$\frac{1+\sqrt{5}}{2}$ 1.618	$\frac{\sqrt{6}+\sqrt{15}}{3}$ 2.107	$\frac{3\sqrt{2}+\sqrt{34}}{4}$ 2.518	...	∞
ϕ	1	$\frac{1+\sqrt{5}}{\sqrt{2}}$ 2.288	$\sqrt{2} + \sqrt{5}$ 3.650	$\frac{3+\sqrt{17}}{\sqrt{2}}$ 5.037	...	∞
ψ	1	$\frac{1+\sqrt{5}}{2\sqrt{2}}$ 1.144	$\frac{\sqrt{2}+\sqrt{5}}{3}$ 1.217	$\frac{3+\sqrt{17}}{4\sqrt{2}}$ 1.259	...	$\sqrt{2}$ 1.414

of vertices as shown in Figs. 7(a) and 7(b). Of the three additional Harriss vertex types, one is new and two appear as derivatives of the Ammann-Beenker vertices. The new vertex is a sequence of two adjacent squares and four consecutive parallelograms, each contributing the acute angle of 45° [yellow circle in Figs. 7(a) and 7(b)]. The first derivative vertex arises because, in the two-length Harriss tiling, the Ammann-Beenker square-square-parallelogram-square-parallelogram vertex splits into two distinct vertices [turquoise and blue circles in Figs. 7(a) and 7(b)]. For the same reason, there exist two variants of the square-parallelogram-parallelogram vertex in the Harriss tiling [lilac and pink circles in Figs. 7(a) and 7(b)]; hence the second derivative vertex.

The two types of square-parallelogram-parallelogram vertices are interesting in view of the random tiling models [26]. In such structures, tile rearrangement shown in Fig. 8 is possible due to the small energy barrier separating the two configurations and can thus be thermally activated. This phason mode is characteristic for quasicrystals [27] and can be regarded as a fluctuation in the perpendicular space.

The canonical boundaries of the perpendicular-space window are determined by conditions such that both points in Fig. 8(a) or 8(b) cannot be inside the window simultaneously. The phason moves in Figs. 8(a) and 8(b) are characterized by vectors $\mathbf{a}_2^{\parallel} - \mathbf{a}_3^{\parallel} + \mathbf{a}_4^{\parallel}$ and $-\mathbf{a}_1^{\parallel} + \mathbf{a}_2^{\parallel} - \mathbf{a}_3^{\parallel}$, respectively. This implies that the sizes of the octagonal window in the horizontal and the vertical directions [Fig. 7(b)] is

$$l_{\text{hv}} = |\mathbf{a}_2^{\perp} - \mathbf{a}_3^{\perp} + \mathbf{a}_4^{\perp}|, \quad (31)$$

whereas that in the diagonal direction is

$$l_{\text{d}} = |-\mathbf{a}_1^{\perp} + \mathbf{a}_2^{\perp} - \mathbf{a}_3^{\perp}|. \quad (32)$$

Figure 9 shows the projection windows of the $k = 2, 4, 6$, and 8 tilings, with all of them colored using the same color code as in Fig. 7(b). For $k = 2$, the window is a regular octagon, whereas for $k = 4, 6, \dots$ the window is an octagon with fourfold symmetry and sides s_k and ℓ_k , with the ratio $\ell_k/s_k = \psi$ tending to $\sqrt{2}$ as $k \rightarrow \infty$. These windows are projections of the four-dimensional hypercuboids onto the perpendicular space.

C. Fourier transforms

To evaluate the Fourier transform of the even-numbered metallic-mean tilings, we first define reciprocal lattice vectors \mathbf{q}^{\parallel} such that $\mathbf{a}_i \cdot \mathbf{q}_j = 2\pi\delta_{ij}$:

$$\mathbf{q} = \sum_{i=1}^4 n_i \mathbf{q}_i \equiv \sum_{i=1,3} n_i \left(\frac{2\pi}{a}\right) \mathbf{e}_i + \sum_{i=2,4} n_i \left(\frac{2\pi}{c}\right) \mathbf{e}_i. \quad (33)$$

Using the projection matrices, we calculate the reciprocal lattice vectors, their lengths being as follows:

$$|\mathbf{q}_{\text{odd}}^{\parallel}| = \frac{2\pi\ell}{a} \sqrt{\frac{1}{\ell^2 + 1}}, \quad (34)$$

$$|\mathbf{q}_{\text{even}}^{\parallel}| = \frac{2\pi}{c} \sqrt{\frac{1}{\ell^2 + 1}}, \quad (35)$$

$$|\mathbf{q}_{\text{odd}}^{\perp}| = \frac{2\pi}{a} \sqrt{\frac{1}{\ell^2 + 1}}, \quad (36)$$

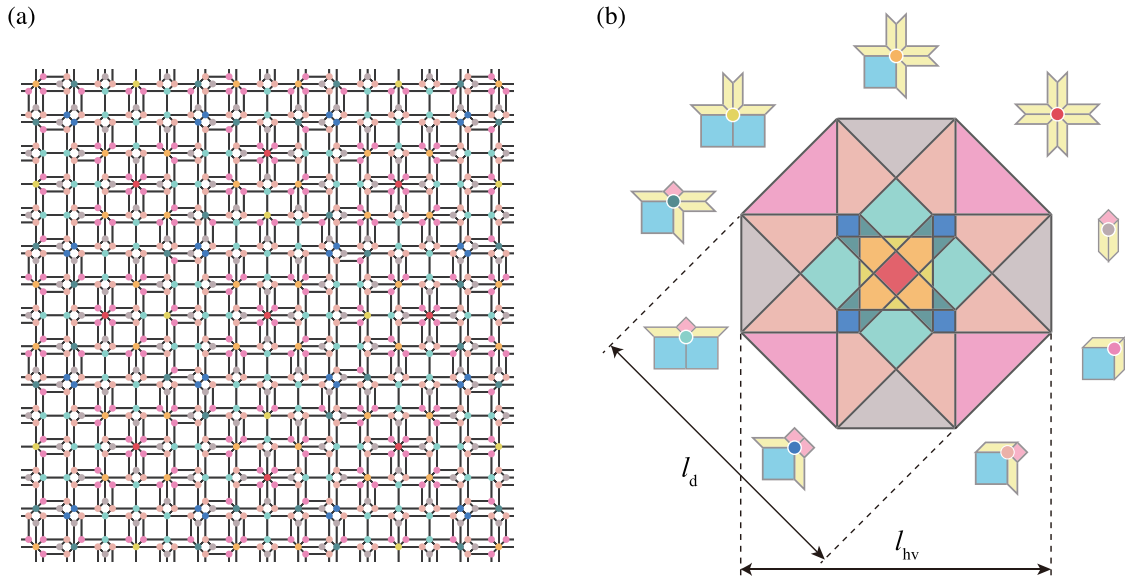


FIG. 7. Local vertex configuration (a) and perpendicular-space structure (b) of the Harriss canonical II tiling; the colored circles decorating each vertex indicate vertex types. In panel (b), the regions of the octagonal projection window are colored according to the type of vertex that they produce, and l_{hv} and l_d denote the size of the window in the horizontal or vertical direction and in the diagonal direction, respectively.

and

$$|\mathbf{q}_{\text{even}}^\perp| = \frac{2\pi\ell}{c} \sqrt{\frac{1}{\ell^2 + 1}}. \quad (37)$$

Thus we have

$$\frac{|\mathbf{q}_{\text{odd}}^\parallel|}{|\mathbf{q}_{\text{even}}^\parallel|} = \frac{c\ell}{a} = \psi, \quad \frac{|\mathbf{q}_{\text{even}}^\perp|}{|\mathbf{q}_{\text{odd}}^\perp|} = \frac{a\ell}{c} = \phi. \quad (38)$$

Figure 10 shows the reciprocal lattice vectors in both physical and perpendicular space for $k = 2, 4, 6$, and ∞ . As k is increased, the four physical-space basis vectors become increasingly less linearly independent and, for $k \rightarrow \infty$, only two of them are: $\mathbf{q}_1^\parallel = \mathbf{q}_2^\parallel - \mathbf{q}_4^\parallel$ and $\mathbf{q}_3^\parallel = \mathbf{q}_2^\parallel + \mathbf{q}_4^\parallel$. Concomitantly, the magnitudes of vectors \mathbf{q}_1^\perp and \mathbf{q}_3^\perp decrease; in the limit $k \rightarrow \infty$, these two vectors vanish.

When computing the Fourier transforms, we rely on the following identity for any pair of vectors in the superspace lattice $\mathbf{x} = (\mathbf{x}^\parallel, \mathbf{x}^\perp)$ and in the corresponding reciprocal lattice $\mathbf{q} = (\mathbf{q}^\parallel, \mathbf{q}^\perp)$: $1 = \exp(i\mathbf{q} \cdot \mathbf{x}) = \exp(i\mathbf{q}^\parallel \cdot \mathbf{x}^\parallel) \exp(i\mathbf{q}^\perp \cdot \mathbf{x}^\perp)$. If particle's positions are described by δ functions so that the density reads $f(\mathbf{r}^\parallel) = \sum_{j=1}^N \delta(\mathbf{r}^\parallel - \mathbf{x}_j^\parallel)$, then the Fourier

transform of the density is calculated as

$$\int d\mathbf{r}^\parallel e^{-i\mathbf{q}^\parallel \cdot \mathbf{r}^\parallel} f(\mathbf{r}^\parallel) = \sum_{j=1}^N e^{-i\mathbf{q}^\parallel \cdot \mathbf{x}_j^\parallel} = \sum_{j=1}^N e^{i\mathbf{q}^\perp \cdot \mathbf{x}_j^\perp}. \quad (39)$$

In the last step, we resorted to the above identity.

Figure 11 shows the simulated diffraction patterns for $k = 2, 4, 6$, and 8 . The computed intensities are normalized by the central peak with indices $(0, 0, 0, 0)$. In Fig. 11(b), which corresponds to the Harriss canonical II tiling, we observe $\beta_4 = \tau^3$ scaling in the horizontal and the vertical directions and the τ scaling in the diagonal directions. For large k such as $k = 8$, the diffraction pattern is similar to the Fourier transform of a square lattice with $1/\beta_k$ scaled satellite peaks. In this respect, our metallic-mean quasicrystals are similar to incommensurate structures showing various satellite peaks, for which the superspace concept has been applied [11]. However, the difference is that these quasicrystals are marked by exact self-similarity characterizing the three basis tiles. To see this self-similarity, a square and a $1/\beta_k$ scaled square are superimposed onto the Fourier transform of

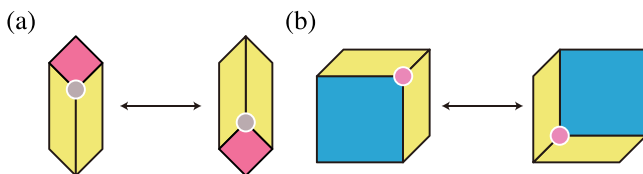


FIG. 8. Phason moves at the square-parallelgram-parallelgram vertex containing SS tile (a) and LS tile (b). This local rearrangement is possible without any changes to the rest of the tiling.

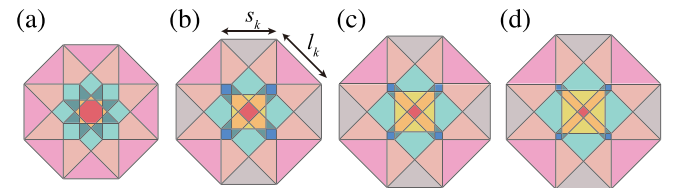


FIG. 9. Projection windows: $k = 2$ [Ammann-Beenker tiling (a)], $k = 4$ [Harriss canonical II tiling (b)], $k = 6$ (c), and $k = 8$ (d). The short and long sides of the projection windows are denoted by s_k and ℓ_k , respectively: The ratio $\ell_k/s_k = \psi$ starts from 1 at $k = 2$ and approaches $\sqrt{2}$ for $k \rightarrow \infty$.

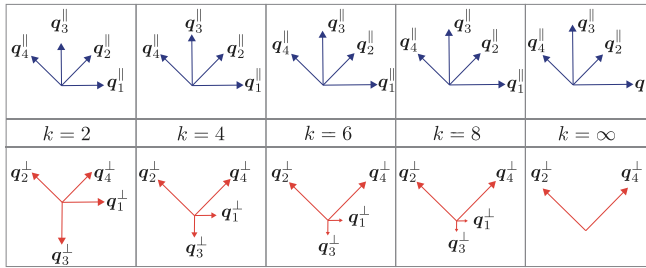


FIG. 10. Reciprocal-space basis vectors \mathbf{q}_j^{\parallel} ($j = 1, 2, 3, 4$) and \mathbf{q}_j^{\perp} ($j = 1, 2, 3, 4$) for $k = 2, 4, 6, 8$, and ∞ . As k is increased, the four physical-space basis vectors become increasingly less linearly independent, whereas \mathbf{q}_1^{\perp} and \mathbf{q}_3^{\perp} shrink in length and, for $k \rightarrow \infty$, only two physical-space basis vectors remain independent.

the $k = 4, 6$, and 8 patterns in Figs. 11(b)–11(d) as guides to the eye.

IV. DISCUSSION

The two-parameter family of the fourfold quasicrystalline pattern proposed here, and especially its subset characterized by even-numbered metallic-mean inflation factors, represents a natural generalization of the eightfold Ammann-Beenker tiling and the fourfold Harriss canonical II tiling. Like the multiple-of-3 [21] and other [18] metallic-mean sixfold quasicrystals, the even-numbered metallic-mean fourfold tilings constitute a sequence of aperiodic approximants of peri-

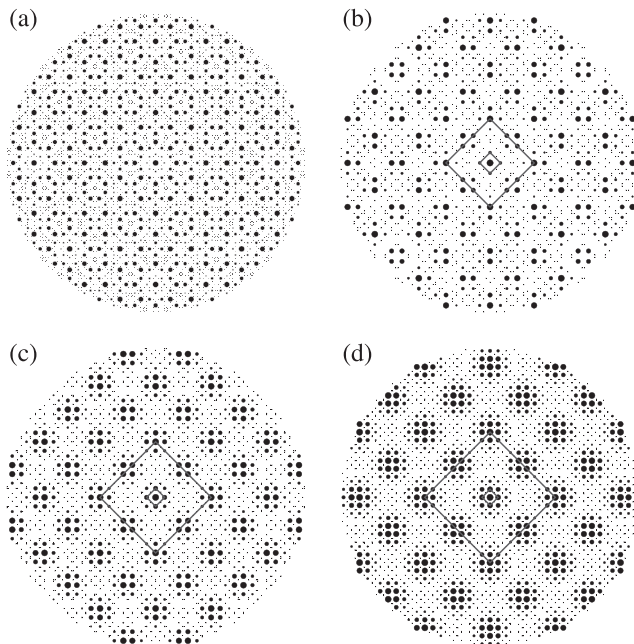


FIG. 11. Fourier transforms of even-numbered metallic-mean tilings: $k = 2$ (a), $k = 4$ (b), $k = 6$ (c), and $k = 8$ (d). The metallic-mean scaling factor β_k is shown by a pair of squares in panels (b)–(d). Spots are normalized relative to the central peak; shown are all spots with intensities $I(\mathbf{q}^{\parallel}) > 0.0045$. A square and a $1/\beta_k$ scaled square are superimposed as guides to the eye in panels (b)–(d).

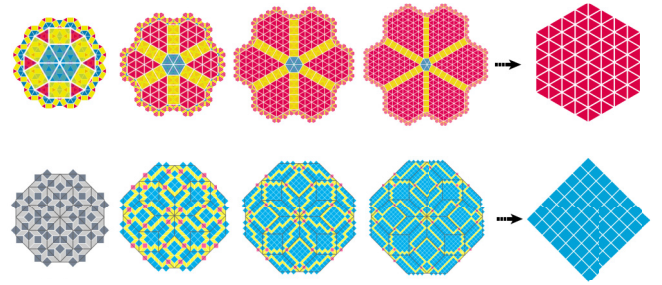


FIG. 12. Alternative type of square aperiodic tilings with even-numbered metallic mean for $k = 2, 4, 6, 8$, and ∞ (bottom row, left to right). Shown are the second-generation tilings and the leftmost diagram is the Ammann-Beenker tiling. The top row contains the type IA hexagonal metallic-mean $k = 3, 6, 9, 12$, and ∞ tilings [21] shown for comparison.

odic crystals, thereby introducing another link between the two kinds of ordered structures. Both square and hexagonal metallic-mean tilings are based on three tiles, two of which are of the same shape. However, there exist several conceptual differences between the hexagonal and the square metallic-mean tilings. In the hexagonal ones, the type IA or IB patterns contain (large) domains consisting of a single tile and can thus be regarded as locally periodic but globally quasiperiodic; as such, they can be viewed as incommensurately modulated structures with an underlying periodic crystal and modulation vectors from a sixfold quasicrystal. On the other hand, the tiles forming our square quasicrystalline patterns are locally mixed. The second difference between the two sequences pertains to the way they approach the periodic crystal in the limit of large inflation ratios: the hexagonal patterns are dominated by a single tile type which outnumbers the other two tile types, whereas in the square patterns the fractions of all tile types remain finite but the area occupied by the majority tile approaches 100%.

In view of these results, we expect that there are many yet unexplored possibilities to devise new substitution tilings of various symmetries and in view of our analysis of the different types of hexagonal metallic-mean tilings at the same inflation ratio [21] we conjecture that, generally, there exist several substitution rules for tilings with the same symmetry and based on the same prototiles—like the five type I hexagonal tilings at $k = 6$. For example, we anticipate that there will be an alternative type of a square tiling characterized by local periodic but global quasiperiodic order, which would be analogous to the type IA and IB hexagonal tilings [21]. Such a square tiling is shown in Fig. 12 together with its hexagonal counterpart.

The last point that we wish to address here deals with these tilings as physical entities. In view of the elaborate structure of square aperiodic approximants, one wonders in what kind of particles it arises. At this point, we cannot provide a specific answer but we note that the range of the interactions needed to stabilize such tilings (more precisely, their random variants) may be considerably shorter than the lengthscale of the large structural features. This expectation is based on the findings of simulations of particles inter-

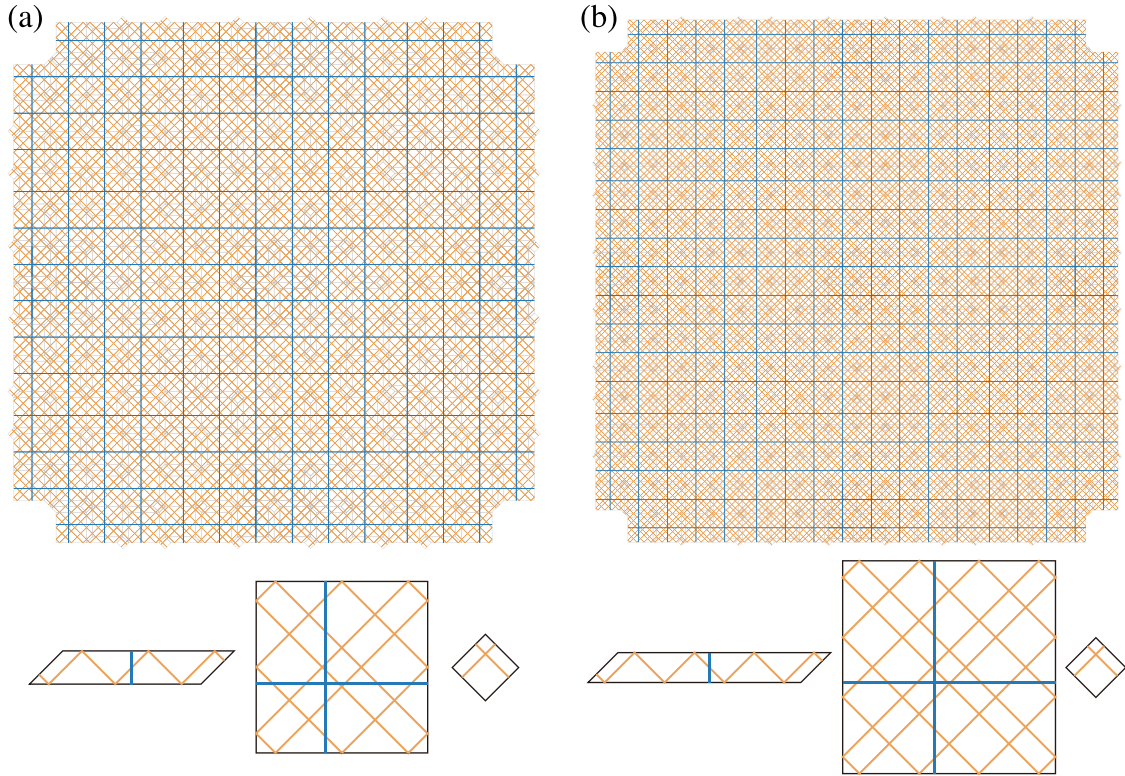


FIG. 13. Ammann lines of the second-generation even-numbered metallic-mean tilings for $k = 6$ and 8 [(a) and (b), respectively]. At first sight, they form square grids, but a careful inspection shows that this is not the case.

acting with a Lennard-Jones–Gauss potential, which were shown to form twin-boundary metallic-mean superstructures on a scale much larger than the nearest-neighbor distance [22], and of hard-core/square-shoulder particles shown to form a host of quasicrystalline phases [28] including the random bronze-mean hexagonal quasicrystal [19]. Furthermore, the bronze-mean quasicrystal and a new hexagonal quasicrystal (type IIC tiling from Ref. [21]) having a larger inflation ratio can be stabilized by complex pair potentials in the scheme of the dynamical density functional theory [20].

By elaborating the subdivision rules, the higher-dimensional representation, and the diffraction patterns of the square aperiodic approximants as well as by discussing their non-metallic-mean variants, we provide a comprehensive description of this particular type of incommensurately modulated structure. As such, our findings offer another perspective of the manifestation of aperiodic approximants with square symmetry.

ACKNOWLEDGMENTS

We thank A. J. Archer, M. Engel, A. Koga, T. Matsubara, and A. M. Rucklidge for fruitful discussions. This project has been supported by the Japan Society for the Promotion of Science through Grant-in-Aid for Scientific Research (C) (No. 19K03777 and No. 24K06982), by the Slovenian Research Agency (research core funding No. P1-0055), as well as by the Japanese-Slovenian bilateral project JPJSBP1 (No. 20195005) and No. BI-JP/19-21-004 co-funded by the Slovenian Research Agency.

APPENDIX : AMMANN LINES

According to Socolar [7], the equations of the Ammann lines can be written as follows: let \mathbf{e}_i^\parallel be defined as $\mathbf{e}_i^\parallel = \cos[(i-1)\pi/4]$ and let $\mathbf{x}_{i,N}$ be a point on the N th line in the grid with lines perpendicular to \mathbf{e}_i^\parallel . Let $\lfloor x \rfloor$ denote the greatest integer less than or equal to x . Then

$$\mathbf{x}_{i,N} \cdot \mathbf{e}_i^\parallel = S^{(\text{odd})} \left(N + a_i + \frac{1}{2\beta_k} + \frac{1}{\beta_k} \left\lfloor \frac{N}{\beta_k} + b_i \right\rfloor \right), \quad (i = 1, 3) \text{ vertical and horizontal}, \quad (\text{A1})$$

$$\mathbf{x}_{i,N} \cdot \mathbf{e}_i^\parallel = S^{(\text{even})} \left(N + a_i + \frac{1}{2\gamma_k} + \frac{1}{\gamma_k} \left\lfloor \frac{N}{\gamma_k} + b_i \right\rfloor \right), \quad (i = 2, 4) \text{ diagonal}, \quad (\text{A2})$$

with

$$a_i = \begin{cases} \frac{1}{2\beta_k} + \mathbf{u} \cdot \mathbf{e}_i^\parallel + p_i + \frac{q_i}{\beta_k}, & (i = 1, 3), \\ \frac{1}{2\gamma_k} + \mathbf{u} \cdot \mathbf{e}_i^\parallel + p_i + \frac{q_i}{\gamma_k}, & (i = 2, 4) \end{cases} \quad (\text{A3})$$

and

$$b_i = \begin{cases} \mathbf{w} \cdot \mathbf{e}_i^\perp - q_i + \frac{p_i}{\beta_k}, & (i = 1, 3), \\ \mathbf{w} \cdot \mathbf{e}_i^\perp - q_i + \frac{p_i}{\gamma_k}, & (i = 2, 4), \end{cases} \quad (\text{A4})$$

where

$$\beta_k = \frac{k + \sqrt{k^2 + 4}}{2}, \quad \gamma_k = \frac{2 + \sqrt{k^2 + 4}}{k}. \quad (\text{A5})$$

Here \mathbf{u} and \mathbf{w} are arbitrary vectors corresponding to the phonon and phason variables and p_i and q_i are arbitrary integers. Note that the expressions contain the same p_i and q_i . In each grid, the sequence of spacings between adjacent lines is a quasiperiodic sequence of two lengths L and S (Fig. 13). The ratio of the two different intervals between the Ammann lines can be written as $1 + 1/\beta_k$ ($i = 1, 3$) and $1 + 1/\gamma_k$ ($i = 2, 4$).

-
- [1] D. Levine and P. J. Steinhardt, Quasicrystals: A new class of ordered structures, *Phys. Rev. Lett.* **53**, 2477 (1984).
- [2] D. Levine and P. J. Steinhardt, Quasicrystals. I. Definition and structure, *Phys. Rev. B* **34**, 596 (1986).
- [3] J. E. S. Socolar and P. J. Steinhardt, Quasicrystals. II. Unit-cell configurations, *Phys. Rev. B* **34**, 617 (1986).
- [4] R. Penrose, The role of aesthetics in pure and applied mathematical research, *Bull. Inst. Maths. Appl.* **10**, 266 (1974).
- [5] A. L. Mackay, Crystallography and the penrose pattern, *Physica A* **114**, 609 (1982).
- [6] P. Stampfli, A dodecagonal quasi-periodic lattice in two dimensions, *Helv. Phys. Acta* **59**, 1260 (1986).
- [7] J. E. S. Socolar, Simple octagonal and dodecagonal quasicrystals, *Phys. Rev. B* **39**, 10519 (1989).
- [8] F. P. M. Beenker, Algebraic theory of non-periodic tilings of the plane by two simple building blocks: a square and a rhombus, EUT report. WSK, Dept. of Mathematics and Computing Science, Technical Report 82-WSK-04 (Eindhoven University of Technology, 1982).
- [9] S. I. Ben-Abraham and F. Gähler, Covering cluster description of octagonal MnSiAl quasicrystals, *Phys. Rev. B* **60**, 860 (1999).
- [10] R. Lifshitz, Quasicrystals: A matter of definition, *Found. Phys.* **33**, 1703 (2003).
- [11] T. Janssen, G. Chapuis, and M. de Boissieu, *Aperiodic Crystals: From Modulated Phases to Quasicrystals* (Oxford University Press, Oxford, 2007).
- [12] M. Baake and U. Grimm, *Aperiodic Order: Volume 1, A Mathematical Invitation* (Cambridge University Press, Cambridge, UK, 2013).
- [13] R. Lifshitz, The square Fibonacci tiling, *J. Alloys Compd.* **342**, 186 (2002).
- [14] S. Coates, J. A. Smerdon, R. McGrath, and H. R. Sharma, A molecular overlayer with the Fibonacci square grid structure, *Nat. Commun.* **9**, 3435 (2018).
- [15] E. O. Harriss and J. S. W. Lamb, Canonical substitutions tilings of Ammann-Beenker type, *Theor. Comput. Sci.* **319**, 241 (2004). See also <https://tilings.math.uni-bielefeld.de/substitution/example-of-canonical-2/>.
- [16] A. Koga and S. Coates, Ferrimagnetically ordered states in the Hubbard model on the hexagonal golden-mean tiling, *Phys. Rev. B* **105**, 104410 (2022).
- [17] S. Coates, R. Lifshitz, A. Koga, R. McGrath, H. R. Sharma, and R. Tamura, Hexagonal and trigonal quasiperiodic tilings, [arXiv:2201.11848](https://arxiv.org/abs/2201.11848) [cond-mat.soft].
- [18] T. Matsubara, A. Koga, A. Takano, Y. Matsushita, and T. Dotera, Aperiodic approximants bridging quasicrystals and modulated structures, *Nat. Commun.* **15**, 5742 (2024).
- [19] T. Dotera, S. Bekku, and P. Ziherl, Bronze-mean hexagonal quasicrystal, *Nat. Mater.* **16**, 987 (2017).
- [20] A. J. Archer, T. Dotera, and A. M. Rucklidge, Rectangle-triangle soft-matter quasicrystals with hexagonal symmetry, *Phys. Rev. E* **106**, 044602 (2022).
- [21] J. Nakakura, P. Ziherl, J. Matsuzawa, and T. Dotera, Metallic-mean quasicrystals as aperiodic approximants of periodic crystals, *Nat. Commun.* **10**, 4235 (2019).
- [22] M. Engel, Entropic stabilization of tunable planar modulated superstructures, *Phys. Rev. Lett.* **106**, 095504 (2011).
- [23] M. Senechal, The mysterious Mr. Ammann, *Math. Intell.* **26**, 10 (2004).
- [24] L. Boyle and P. J. Steinhardt, Coxeter pairs, Ammann patterns, and Penrose-like tilings, *Phys. Rev. B* **106**, 144113 (2022).
- [25] J. E. S. Socolar, Weak matching rules for quasicrystals, *Commun. Math. Phys.* **129**, 599 (1990).
- [26] V. Elser, Comment on “Quasicrystals: A new class of ordered structures”, *Phys. Rev. Lett.* **54**, 1730 (1985).
- [27] J. E. S. Socolar, T. C. Lubensky, and P. J. Steinhardt, Phonons, phasons, and dislocations in quasicrystals, *Phys. Rev. B* **34**, 3345 (1986).
- [28] T. Dotera, T. Oshiro, and P. Ziherl, Mosaic two-lengthscale quasicrystals, *Nature (London)* **506**, 208 (2014).